Review

A Review of Geological Applications of High-spatial-resolution Remote Sensing Data

Chunming Wu [1], Xiao Li[1,*], Weitao Chen[2,*] , Xianju Li[2]

[1] Geological Survey Insitute, China University of Geosciences, Wuhan 430074, China; wcmcug@cug.edu.cn
[2] Faculty of Computer Science, China University of Geosciences, Wuhan 430074, China; ddwhlxj@cug.edu.cn
* Correspondence: wtchen@cug.edu.cn; cuglx@foxmail.com; TEL: +86-138-7157-1861, +86-132-9668-4768.

Abstract: Geologists employ high-spatial-resolution (HR) remote sensing (RS) data for many diverse applications as they effectively reflect detailed geological information, enabling high-quality and efficient geological surveys. Applications of HR RS data to geological and related fields have grown recently. By analyzing these applications, we can better understand the results of previous studies and more effectively use the latest data and methods to efficiently extract key geological information. HR optical remote sensing data are widely used in geological hazard assessment, seismic monitoring, mineral exploitation, glacier monitoring, and mineral information extraction due to high accuracy and clear object features. Compared with optical satellite images, synthetic-aperture radar (SAR) images are stereoscopic and exhibit clear relief, strong performance, and good detection of terrain, landforms, and other information. SAR images have been applied to seismic mechanism research, volcanic monitoring, topographic deformation, and fault analysis. Furthermore, a multi-standard maturity analysis of the geological applications of HR images using literature from the Science Citation Index reveals that optical remote sensing data are superior to radar data for mining, geological disaster, lithologic, and volcanic applications, but inferior for earthquake, glacial, and fault applications. Therefore, geological remote sensing research needs to be truly multidisciplinary or interdisciplinary, ensuring more detailed and efficient surveys through cross-linking with other disciplines. Moreover, the recent application of deep learning technology to remote sensing data extraction has improved automatic processing and data analysis capabilities.

Keywords: High-spatial-resolution images; Geology; Deep learning; Remote sensing

Preprints (www.preprints.org) | NOT PEER-REVIEWED | Posted: 7 November 2018 doi:10.20944/preprints201811.0162.v1

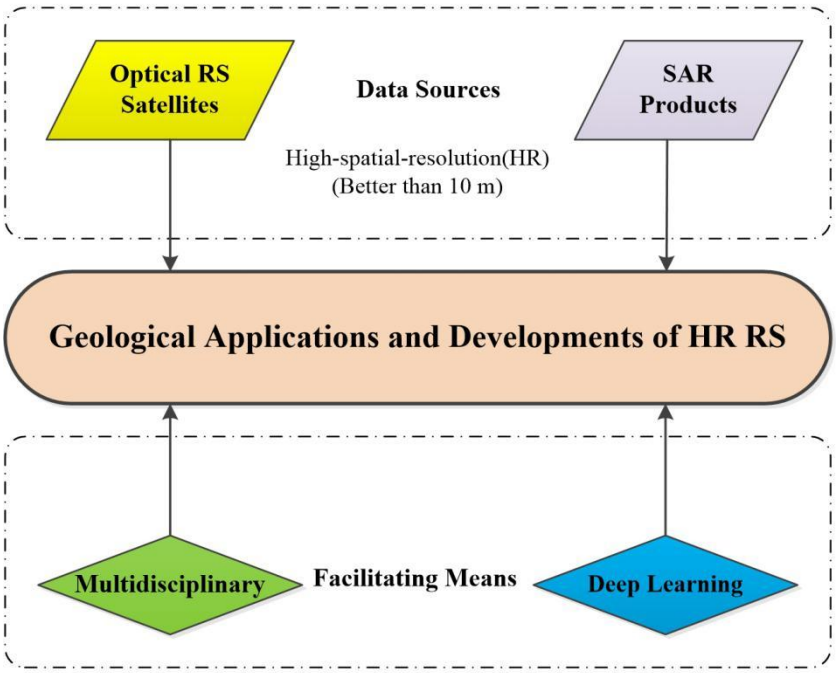

Graphical Abstract

Contents

Preprints (www.preprints.org) | NOT PEER-REVIEWED | Posted: 7 November 2018 doi:10.20944/preprints201811.0162.v1

1. Introduction

Geology has an increasingly important role in protecting the eco-environment and providing land and mineral resources. The various categories of geological survey include: using different methods and different content for geological mapping at various scales, regional geophysical survey, regional geochemical investigation, remote sensing (RS) geological survey and evaluation, strategic mineral evaluation, regional environmental geological survey, and marine geological survey. With the development of RS technology, geologists have used these data for mineral identification and mapping, regional mapping, mineral resource exploration, mining environment monitoring, and oil and gas leakage monitoring. RS is a proven technique that can be confidently and efficiently applied in almost all disciplines of Earth science [1,2,3,4,5,6,7,8,9,10,11,12,13,14,15,16,17,18,19], for example:

(i) Geological information and remote sensing data provide information about Earth's surface structure [20]. Because of the range of geological hazards and poor natural conditions, traditional geological surveys of geological hazards are very complex. Therefore, high-resolution (HR) remote sensing plays an important role in geological hazard investigations.

(ii) The global use of RS for the mapping of regional structures has a long history [21,22,23]. Recent advances in GIS spatial tools and the availability of various remotely sensed data have enabled the reliable delineation of topographical boundaries [24]. Additionally, high-spatial-resolution topographic data are a crucial prerequisite for evaluating and modeling volcanic hazards [25].

(iii) As a cutting-edge technology currently supporting the geosciences (among other disciplines), RS could play a significant role in mineral exploration research, effectively decreasing initial investments and saving time by targeting the most likely locations of ore deposits [26].

Compared to field investigations, surveying alteration minerals using RS imagery is more economical and convenient due to reduced labor costs [27]. HR can provide more sophisticated geological surveys that incorporate structural interpretations, lithology, metallogenic or ore-controlling elements, regional mineral resources, and lithology-structure remote sensing interpretation maps.

Currently, there are many published reviews of RS applications in geology. Most of these reviews are related to the geological applications of hyperspectral remote sensing [28,29,30,31,32,33,34,35,36], with fewer studies involve optical and radar geological remote sensing at high spatial resolution [37,38], despite the fact that HR RS data can be beneficial for many different types of geological research. Thus, the objectives of this review are as follows: (i) analyze various HR remote sensing techniques and their applications; specifically optical satellite remote sensing and synthetic aperture radar (SAR); (ii) provide a geological application maturity analysis of HR images for reference to different research fields; and (iii) propose future research directions including multidisciplinary approaches and deep learning techniques.

2. Optical satellite remote sensing products and geological applications

In recent years, HR optical remote sensing satellite technology has developed rapidly, exhibiting continuously increasing resolution and more diverse imaging modes. HR satellite imagery provides a useful source for mapping the Earth's surface [39,40,41]; civil optical remote sensing satellites with a spatial resolution of better than 10 m have appeared in recent years (Table 1).

2.1 SPOT satellites

 doi:10.20944/preprints201811.0162.v1

The SPOT family of optical satellites better reflects the attribute information of vegetation, rock, soil, water bodies, ice bodies, and linear structures, among others, which greatly improves the accuracy of judgment and interpretation. SPOT images have been used as base maps for tracing and constructing detailed geological maps of prospect and target areas [42]. Among these satellites, SPOT-5/6/7 data has played an important role in geology. Some key geology applications are as follows:

(i) Lithology: geologists have used SPOT images to extract lithologic information and predict bedrock geology mapping [43,44].

(ii) Glaciology: studying the effects of global warming on mountainous and polar glaciers is an effective use of stereo imaging capability [45,46,47].

(iii) Topography: the stereo imaging model of SPOT HRS improves high spatial mapping and high-resolution digital elevation model (DEM) generation [48,49,50,].

(iv) Geological disasters: high-resolution multispectral and panchromatic images significantly help the artificial and automatic mapping of geological hazards and their comparisons for the prediction and prevention of geological hazards [51,52,53,54,55].

(v) Mine ecology: high-spatial-resolution SPOT data is an important reference for monitoring the accumulation of mine solid waste and ecological restoration in mining exploitation areas [56,57,58].

 doi:10.20944/preprints201811.0162.v1

Table 1. Civil optical satellite data with a spatial resolution of more than 10 m used for geological remote sensing surveys in recent years.

No.	Satellite name	Emission time	Sensor type	Spatial resolution (m)		Stereoscopic imaging capability	Country
				Pan	Ms		
1	Jilin-1-03	2017/01/9	3Ms	—	0.92	NO	China
2	SuperView-1	2016/12/29	Pan+5Ms	0.5	2	NO	China
3	WorldView-4	2016/11/11	Pan+4Ms	0.31	1.24	YES	USA
4	ZiYuan-3-02	2016/05/30	Pan+4Ms	2.1	5.8	YES	China
5	Mapping Satellite-1-03	2015/10/26	Pan+4Ms	2	10	YES	China
6	Jilin-1-A	2015/10/7	Pan+3Ms	0.72	2.88	NO	China
7	Beijing-2	2015/07/11	Pan+4Ms	＜1	3.2	NO	China
8	Sentinel-2	2015/06/23	13Ms	—	10	NO	EU
9	CBERS-04	2014/12/7	Pan+4Ms	5	10	NO	China
10	Gaofen-2	2014/08/19	Pan+4Ms	1	4	NO	China
11	WorldView-3	2014/08/13	Pan+16Ms	0.31	1.24/3.7	YES	USA
12	SPOT 7	2014/06/30	Pan+4Ms	1.5	8	YES	France
13	DEIMOS-2	2014/06/19	Pan+4Ms	0.75	3	NO	Spain
14	KazEOSat-1	2014/04/30	Pan+4Ms	1	4	NO	Kazakhstan
15	OFEQ 10	2014/04/9	Pan	0.5	—	NO	Israel
16	Planet Labs	2014/01/17	3Ms	—	3/3.7	NO	USA
17	DubaiSat-2	2013/11/21	Pan+4Ms	1	4	NO	UAE
18	Gaofen-1	2013/04/26	Pan+4Ms	2	8	NO	China
19	SJ-9	2012/10/14	Pan+4Ms	2.5	10	NO	China
20	SPOT 6	2012/09/9	Pan+4Ms	1.5	8	YES	France
21	KompSat-3	2012/05/17	Pan+4Ms	0.7	2.8	NO	Korea

 doi:10.20944/preprints201811.0162.v1

22	Mapping Satellite-1-02	2012/05/6	Pan+4Ms	2	10	YES	China
23	ZiYuan-3	2012/01/9	Pan+4Ms	2.1	6	YES	China
24	CBERS-02C	2011/12/22	Pan+3Ms	5/2.36	10	NO	China
25	Pleiades-1	2011/12/17	Pan+4Ms	0.5	2	NO	France
26	OFEQ 9	2010/06/22	Pan	0.7	—	NO	Israel
27	WorldView-2	2009/10/6	Pan+8Ms	0.5	1.8	NO	USA
28	Geoeye-1	2008/09/6	Pan+4Ms	0.41	1.65	NO	USA
29	WorldView-1	2007/09/18	Pan	0.51	—	NO	USA
30	CBERS-02B	2007/09/9	Pan+5Ms	2.36	20	NO	China
31	KompSat-2	2006/07/28	Pan+4Ms	1	4	NO	Korea
32	Resurs DK 1	2006/06/15	Pan+3Ms	1	2	NO	Russia
33	EROS-B	2006/04/25	Pan	0.7	—	NO	Israel

Relative Sensor types: Pan= Panchromatic band; Ms= Multispectral band

Preprints (www.preprints.org) | NOT PEER-REVIEWED | Posted: 7 November 2018 doi:10.20944/preprints201811.0162.v1

2.2 WorldView satellites

WorldView satellites have modern geo-positioning accuracy and excellent response capability, can quickly aim at the target to be photographed, and effectively performs stereoscopic imaging in the same orbit. Due to its advantages of fine spectral and spatial features, WorldView data has been widely used in:

(i) Mineralogy: WorldView data is widely used to extract mineral alteration information, evaluate lithologic mapping data, and map minerals because of its high spectral resolution [59,60,61,62].

(ii) Gas detection; i.e. detection of alteration caused by gas leakage using ASTER and WorldView-2 data [63].

(iii) Topography: using the stereo imaging capability of WorldView, researchers can update topographic maps and generate DEMs [64].

(iv) Mining: Worldview-2 satellite imagery has been used to search for ancient gold mines in the Filippoi area of Macedonia, Greece [65].

(v) Glaciology: researchers have determined the 3D variation and seasonal velocity evolution of glaciers using the stereo imaging capability of WorldView data [66,67],.

Compared with TM and ASTER data, WorldView-3 data have a higher spatial, spectral, and radiation resolution and more potential for remote sensing applications related to the extraction of alteration information [68]. After determining the mapping relationship between WorldView remote sensing data and the field, it is possible to clearly identify the lithofacies and belts of various strata, lithologic segments, subdivisions of intrusions, and volcanic rocks, and accurately judge the scale, morphology, and active period of various geological structures [60]. Therefore, we can use WorldView data to implement HR remote sensing interpretation indicators for lithology, tectonics, and ore controlling elements.

2.3 Chinese survey satellites

The ZiYuan-3 remote sensing satellite was the first civil high-resolution stereo mapping satellite in China, which can establish digital surface models (DSMs) and DEMs with high precision. It is suitable for obtaining detailed information of micro-geomorphological features and can accurately reflect the linear image features of minor secondary fault structures [69]. ZY-3 data have been widely applied in surveying and mapping, agriculture, forestry, environmental protection, disaster reduction, urban planning, and other fields [70]. ZY-3 has also been used to conduct land cover mapping in surface-mined areas [40,41,71]. For some high mountainous areas, ZY-3 data cannot meet the corresponding accuracy requirements, and only existing topography and geological maps can be repaired and updated. Table 2 presents some recent examples of ZY-3 satellite geological applications.

Table 2. Published literature on the geological applications of ZY-3 data in recent years.

Research field	Author, publishing date	Paper topic	Data source	Resolution (m)	Related literature
Topography	Dong et al., 2016	DEM	ZY-3	2.1	Assessment of orthoimages and DEMs derived from ZY-3 stereo images in Northeastern China
	Zheng et al., 2016	DEM	ZY-3 & GF-1	2.1	DEM-aided bundle adjustment with multisource satellite imagery: ZY-3 and GF-1 over large areas

Preprints (www.preprints.org) | NOT PEER-REVIEWED | Posted: 7 November 2018 doi:10.20944/preprints201811.0162.v1

	Zhang et al., 2012	DEM	ZY-3	2.1	DEM extraction and accuracy assessment based on ZY-3 stereo images
Geological disaster	He et al., 2018	Snowmelt flood	ZY-3&HJ-1	2.1	Direct tangible damage assessment for regional snowmelt flood disasters with HJ-1 and HR satellite images: a case study of the Altay region, northern Xinjiang, China
	Chen et al., 2017	Landslide	ZY-3	2.1	Object-oriented landslide mapping using ZY-3 satellite imagery, random forest, and mathematical morphology for the three-gorges reservoir, China
	Lina et al., 2014	Landslide	ZY-3	2.1	Landslide stability evaluation in the three-gorges reservoir using ZY-3 data
Earthquake	Wang et al., 2015	Earthquake monitoring	ZY-3	2.1	Earthquake monitoring for multi-temporal images of Ziyuan-3
Mine	Chen et al., 2018	Land cover classification in complex surface-mined landscapes	ZY-3	2.1	Assessing different feature sets' effects on land cover classification in complex surface-mined landscapes by Ziyuan-3 satellite imagery
	Li et al., 2016	Mapping of complex surface-mined and agricultural landscapes	ZY-3	2.1	A comparison of machine learning algorithms for mapping of complex surface-mined and agricultural landscapes using Ziyuan-3 stereo satellite imagery

2.4 Sentinel-2

The Sentinel-2 satellite has been widely used for agriculture and forestry planting, determining land cover and forests, monitoring glaciers, and mapping natural disasters. Moreover, the characteristics of the Sentinel-2 band have been employed to determine useful band ratios for extracting important reference minerals. Comparing the band ratio products of ferric iron, ferrous iron, laterite, gossan, ferrous silicate, and ferric oxides to a local geologic map of an imaged hydrothermal area (the Rodalquilar mining area, Cabo de Gata volcanic field, SE Spain) revealed that band ratio products supported the existing conceptual geologic model of the epithermal deposit [72]. The band ratio method of Sentinel-2 data also has great potential for mapping of glacial outlines and performing velocity measurements [73,74]. Additionally, the results of Hyperion/OLI and EnMAP/Sentinel-2 have been compared for mine waste monitoring [75]. Because Sentinel-2 bands (bandwidth included) cover 59% of the identified useful hyperspectral bands and multispectral aims, they can play a key role in the enhancement of hyperspectral data and increase potential applications because of their complementary spatial, temporal, and spectral resolutions [76].

Preprints (www.preprints.org) | NOT PEER-REVIEWED | Posted: 7 November 2018 doi:10.20944/preprints201811.0162.v1

Table 3. Sentinel-2A spectral information [72].

Feature	Sentinel-2A MSI
Hydroxyl bearing alteration	Band 11 / Band 12
All iron oxides	Band 4 / Band 2
Ferrous iron oxides	Band 4 / Band 11
Ferric iron, Fe^{3+}	Band 4 / Band 3
Ferrous iron, Fe^{2+}	Band 8 / Band 12 + Band 3 / Band 4
Laterite	Band 11 / Band 12
Gossan	Band 11 / Band 4
Ferrous silicates	Band 12 / Band 11
Ferric oxides	Band 11 / Band 8
Vegetation	Band 8 / Band 4
NDVI	Band (8-4) / Band (8+4)

3. Synthetic aperture radar (SAR) products and geological applications

While spatial and spectral information is extracted by optical remote sensing, radar remote sensing in the microwave frequency band also provides an irreplaceable source of information for HR Earth observations with both day and night imaging capability [77](Park, 2015). SAR images can provide a wealth of geological and mineral information such as geological structure, lithology, and hidden geological bodies, especially related to volcanic deposits, meteorite impacts, and large faults [78,79,80,81]. The real time quantitative measurement of crustal deformation can be obtained by using ground Sentinel-1 images obtained at different times. In fact, the analysis of Sentinel-1 data has become routine by participating national and international agencies in seismic research, earthquake disaster assessment, and civil defense activities. The main aspects of earthquake analysis using Sentinel-1 data include:

(i) Location and evaluation of hypocenters [82].

(ii) Location and evaluation of induced secondary disasters (landslides, mudslides, seaquakes, surface cracks, surface collapses) [83].

(iii) Estimation of the short-term spatial evolution of seismic sequences [84].

The use of SAR to monitor surface deformation and geological disasters has become a key issue in recent years [85]. This method, which is suitable for large-scale ground deformation, has been widely used in urban surface monitoring, mine surface monitoring, dam peripheral surface monitoring, and other geological conditions. Recent studies employing SAR data with a spatial resolution of greater than 10 m are listed in Table 4.

Preprints (www.preprints.org) | NOT PEER-REVIEWED | Posted: 7 November 2018 doi:10.20944/preprints201811.0162.v1

Table 4. Recent literature on SAR data with a spatial resolution above 10 m and their geological applications.

Research field	Author, publishing date	Paper topic	Data source	Resolution (m)	Related literature
Earthquake	Yun et al., 2017	Rapid damage mapping	COSMO-SkyMed and ALOS-2	1	Rapid damage mapping for the 2015 Mw 7.8 Gorkha earthquake, Nepal, using synthetic aperture radar data from COSMO-SkyMed and ALOS-2 Satellites
	Natsuaki et al., 2016	SAR interferometry	ALOS-2/PALSAR-2	1	SAR interferometry using ALOS-2 PALSAR-2 data for the Mw 7.8 Gorkha earthquake
	Himematsu et al., 2016	Fault source model	ALOS-2/PALSAR-2	1	Fault source model for the 2016 Kumamoto earthquake sequence based on ALOS-2/PALSAR-2 pixel-offset data: evidence for dynamic slip partitioning (EPSP-D-16-00163)
	Marco et al., 2015	Co-seismic liquefaction phenomenon analysis	COSMO-SkyMed	1	Co-seismic liquefaction phenomenon analysis by COSMO-SkyMed: 2012 Emilia (Italy) earthquake
	Mahdi et al., 2015	Post-seismic ground deformation	TerraSAR-X, COSMO-SkyMed, and ALOS	1	Post-seismic ground deformation following the September 2010 Darfield earthquake, New Zealand, from TerraSAR-X, COSMO-SkyMed, and ALOS InSAR
	Fujiwara et al., 2015	Small-displacement linear surface ruptures	ALOS-2	2.5	Small-displacement linear surface ruptures of the 2016 Kumamoto earthquake sequence detected by ALOS-2 SAR interferometry
	Fielding et al., 2013	Kinematic fault slip evolution source models	ALOS and ENVISAT	10	Kinematic fault slip evolution source models of the 2008 M7.9 Wenchuan earthquake in China from SAR interferometry, GPS and teleseismic analysis and implications for Longmen Shan tectonics
	Sato et al., 2012	Analysis of tsunami damage	ALOS PALSAR	2.5	Polarimetric SAR analysis of tsunami damage following the March 11, 2011 East Japan Earthquake

 doi:10.20944/preprints201811.0162.v1

	Brunner et al., 2010	Building damage assessment	QuickBird, WorldView-1 , TerraSAR-X and COSMO-SkyMed	1	Earthquake damage assessment of buildings using VHR optical and SAR imagery
	Guo et al., 2010	Earthquake synergic analysis	Radarsat-2	3	Yushu earthquake synergic analysis using multimodal SAR datasets
	Sun et al., 2008	Synthetic normal faulting	ENVISAT	10	Synthetic normal faulting of the 9 January 2008 Nima (Tibet) earthquake from conventional and along-track SAR interferometry
	Pathier et al., 2006	Displacement field and slip distribution	ENVISAT	10	Displacement field and slip distribution of the 2005 Kashmir earthquake from SAR imagery
Volcano	Saepuloh et al., 2015	Identifying surface materials on an active volcano	ALOS PALSAR	2.5	Identifying surface materials on an active volcano by deriving dielectric permittivity from polarimetric SAR data
	Min-Jeong et al., 2015	Measurement of three-dimensional surface deformation	Cosmo-SkyMed	1	Measurement of three-dimensional surface deformation by Cosmo-SkyMed X-band radar interferometry: Application to the March 2011 Kamoamoa fissure eruption, Kilauea Volcano, Hawai'i
	Champenois et al., 2014	Large-scale inflation of Tungurahua volcano (Ecuador)	ENVISAT	10	Large-scale inflation of Tungurahua volcano (Ecuador) revealed by Persistent Scatterers SAR interferometry
	Martino et al., 2012	On the fractal nature of volcano morphology analysis	TerraSAR-X and COSMO-SkyMed	1	On the fractal nature of volcano morphology detected via SAR image analysis: the case of the Somma-Vesuvius Volcanic Complex
	Heleno et al., 2009	Seasonal tropospheric	ENVISAT	10	Seasonal tropospheric influence on SAR interferograms near the ITCZ – the case of Fogo Volcano and Mount Cameroon

 doi:10.20944/preprints201811.0162.v1

		influence on SAR interferograms near the ITCZ			
	Scharrer et al., 2008	Imprints of sub-glacial volcanic activity on a glacier surface	ERS-1/2, JERS-1 and RADARSAT	10	Imprints of sub-glacial volcanic activity on a glacier surface—SAR study of Katla volcano, Iceland
Mining	Ng et al., 2017	Monitoring subsidence induced by longwall mining activity	Radarsat-2, Sentinel-1 and ALOS-2	1	Satellite radar interferometry for monitoring subsidence induced by longwall mining activity using Radarsat-2, Sentinel-1, and ALOS-2 data
	Yan et al., 2016	Large deformation monitoring over a coal mining region	Radarsat-2	3	Large deformation monitoring over a coal mining region using pixel-tracking method with high-resolution Radarsat-2 imagery
	Bingqian et al., 2015	Monitoring of large gradient deformation in a coal mining area	TerraSAR-X	1	Combining SAR interferometric phase and intensity information for monitoring of large gradient deformation in a coal mining area
	Liu et al., 2014	Monitoring deformations caused by mining	ALOS, ENVISAT and TerraSAR-X	1	Evaluation of InSAR and TomoSAR for monitoring deformations caused by mining in a mountainous area with high-resolution satellite-based SAR
	Zhao et al., 2014	Mining collapse monitoring	ERS-1, Envisat ASAR, TerraSAR-X	1	Mining collapse monitoring with SAR imagery data: a case study of Datong mine, China
	Herrera et al., 2010	Mapping ground movements in open pit mining areas	ERS and ENVISAT	10	Mapping ground movements in open pit mining areas using differential SAR interferometry
	Linlin et al., 2007	Mine subsidence monitoring	ERS-1, ERS-2, JERS-1,	10	Mine subsidence monitoring using multi-source satellite SAR images

 doi:10.20944/preprints201811.0162.v1

			RADARSAT-1 and ENVISAT		
Glacier	Sun et al., 2018	Mapping glacier elevations and changes	TerraSAR-X	1	Mapping glacier elevations and their changes in the Western Qilian Mountains, Northern Tibetan Plateau, by bistatic InSAR
	Pietro et al., 2017	Short-term grounding zone dynamics	COSMO-SkyMed	1	On the short-term grounding zone dynamics of Pine Island Glacier, West Antarctica, observed with COSMO-SkyMed interferometric data
	Liu et al., 2016	Glacier elevation changes	TerraSAR-X	10	Glacier elevation changes (2012–2016) of the Puruogangri Ice Field on the Tibetan Plateau derived from bi-temporal TanDEM-X InSAR data
	Papasodor et al., 2016	Stereo radargrammetry for the generation of glacier DEMs	RADARSAT-2	3	Potential of RADARSAT-2 stereo radargrammetry for the generation of glacier DEMs
	de Andrade et al., 2016	Classification of ice-free areas and glacier facies	Cosmo-SkyMed	1	Cosmo-SkyMed X-band SAR data for classification of ice-free areas and glacier facies on Potter Peninsula, King George Island Antarctica
	Schellenberger et al., 2016	An inter-comparison of techniques for determining velocities of maritime arctic glaciers	RADARSAT-2	3	An inter-comparison of techniques for determining velocities of maritime arctic glaciers, Svalbard, using Radarsat-2 wide fine mode data
	Han et al., 2013	Estimation of annual variation in ice extent and flow velocity of Campbell Glacier	COSMO-SkyMed	1	Estimation of annual variation in ice extent and flow velocity of Campbell Glacier in East Antarctica using COSMO-SkyMed SAR images

Preprints (www.preprints.org) | NOT PEER-REVIEWED | Posted: 7 November 2018 doi:10.20944/preprints201811.0162.v1

	Kumar et al., 2011	Glacier surface velocity estimation	ERS-1/2	3	Glacier surface velocity estimation using SAR interferometry applying ascending and descending passes in the Himalayas
	Zhou et al., 2011	Movement estimate of the Dongkemadi Glacier	ERS-1/2 and ALOS	1	Movement estimate of the Dongkemadi Glacier on the Qinghai-Tibetan Plateau using L-band and C-band spaceborne SAR data
	Huang et al., 2011	Deriving glacier velocity with feature tracking	ALOS	1	Comparison of SAR and optical data in deriving glacier velocity with feature tracking
	Ciappa et al., 2010	Glacier flow estimation	COSMO-SkyMed and SAR-X	1	Perito Moreno Glacier (Argentina) flow estimation by COSMO SkyMed sequence of high-resolution SAR-X imagery
Topography	Tseng et al., 2017	Reconstruction of time-varying tidal flat topography	Jason-2 and ENVISAT	1	Reconstruction of time-varying tidal flat topography using optical remote sensing imageries
	Zhang et al., 2017	Mechanisms of SAR imaging of shallow water topography	ERS-2 and ENVISAT	10	Mechanisms of SAR imaging of shallow water topography of the Subei Bank
	Bian et al., 2017	Underwater topography detection	RADARSAT-2	4	Underwater topography detection in coastal areas using fully polarimetric SAR data
	Meyer et al., 2012	Topography and change detection of Venus	ERS-ENVISAT	1	SAR interferometry of Venus for topography and change detection
	Rodriguez-Cassola et al., 2011	Efficient time-domain image formation with precise topography	TerraSAR-X and F-SAR	1	Efficient time-domain image formation with precise topography accommodation for general bistatic SAR configurations

Preprints (www.preprints.org) | NOT PEER-REVIEWED | Posted: 7 November 2018 doi:10.20944/preprints201811.0162.v1

	Niedermeier et al., 2005	Topography and morphodynamics	ENVISAT	10	Topography and morphodynamics in the German Bight using SAR and optical remote sensing data
Fault	Feng et al., 2017	New evidence for fault segments ruptured in the 2008 Wenchuan Earthquake	ALOS	10	Which fault segments ruptured in the 2008 Wenchuan Earthquake and which did not? New evidence from near-fault 3D surface displacements derived from SAR image offsets
	Ilieva et al., 2016	Fault plane modeling	ENVISAT	10	Fault plane modeling of the 2003 August 14 Lefkada Island (Greece) earthquake based on the analysis of ENVISAT SAR interferograms
	Feng et al., 2013	Fault constraints provided by multiple SAR techniques	ALOS PALSAR	1	The 2011 M-W 6.8 Burma earthquake: fault constraints provided by multiple SAR techniques
	Fielding et al., 2013	Fault-slip source models	ALOS and ENVISAT	1	Fault-slip source models for the 2011 M 7.1 Van earthquake in Turkey from SAR interferometry, pixel offset tracking, GPS, and seismic waveform analysis
	Currenti et al., 2012	Relationship between seismic activation of the Pernicana fault system and volcanic unrest	ALOS and COSMO-SkyMed	1	Modeling of ALOS and COSMO-SkyMed satellite data at Mt Etna: Implications on relation between seismic activation of the Pernicana fault system and volcanic unrest
	Jolivet et al., 2012	Shallow creep on the Haiyuan Fault (Gansu, China)	ENVISAT	10	Shallow creep on the Haiyuan Fault (Gansu, China) revealed by SAR interferometry

Preprints (www.preprints.org) | NOT PEER-REVIEWED | Posted: 7 November 2018 doi:10.20944/preprints201811.0162.v1

4. Discussion and conclusions

4.1 Maturity analysis of geological applications with high resolution remote sensing data

High-spatial-resolution optical remote sensing satellite data exhibit higher resolution and more visual image information than spaceborne synthetic aperture radar data, which simplifies the interpretation and identification of geological information. Compared with optical satellite images, SAR images are stereoscopic and exhibit clear relief, strong performance, and good detection effects for terrain, landforms, and other information. The application of SAR images is highly sensitive to differences in surface morphology and roughness; thus, most radar data are still used in deserts and other low-vegetation coverage areas. The fusion of radar and optical images would significantly simplify the process of target detection and recognition and improve the accuracy of recognition by combining the advantages of both methods.

Table 5 summarizes the results of a maturity analysis of geological applications for HR remote sensing data, scaled between "low" and "high". This maturity assessment is based on a multi-standard analysis of 15 years of relevant literature from the Science Citation Index. The criteria include the quality of the high-resolution data set; i.e., the number of samples selected, the research method, the accuracy of the research results, the number of research reports, and the applicability of the field investigation. Each standard is assigned and weighted equally to obtain a final rating.

Table 5. Maturity [a] of geological applications with high-resolution remote sensing data.

Geological application	Radar	Optical
Geological disasters	Medium-high	High
Earthquake	High	Medium-high
Mine	Medium-high	High
Glacier	High	Low-medium
Topography	Low-medium	Low
Fault	High	Low
Lithology	Low	High
Volcano	Low-medium	Medium-high

[a] Maturity (1–5)= weighted average of quality scores for the high-resolution data set, based on the number of samples selected, the research method, the accuracy of the research results, the number of research reports, and the applicability of the field investigation. Low = 1, low-medium= 2, medium = 3, medium-high = 4, and high = 5.

4.2 Multidisciplinary approaches

Remote sensing as a tool for geological survey also has some limitations because remote sensing images mainly reflect surface information or shallow information, while most geological bodies, geological structures, and geological phenomena reflect three-dimensional information. The integration of geological, remote sensing and geophysical data limits the quantitative details of unknown regions, which can reduce the ambiguity of geological interpretation and improve the accuracy [86,87,88,89,90,91,92,93,94]. In addition, monitoring and understanding of geological processes also requires multidisciplinary analysis and integration of remote sensing data with field observations and underground geophysical data [30]. Using GIS, grid and vector data extracted from the field can be combined with remote sensing, geophysics, and geochemistry data analysis, which can comprehensively analyze

Preprints (www.preprints.org) | NOT PEER-REVIEWED | Posted: 7 November 2018 doi:10.20944/preprints201811.0162.v1

different data types and their relationships, thus laying a foundation for geological analysis. This is an important trend in remote sensing geology; however, it is not always possible to benefit from these advantages and new technical insights.

The combination of high-resolution remote sensing data and traditional medium-low-resolution remote sensing data (ETM and ASTER) can be used to understand geological structures and mineralization from a new perspective. It not only takes advantage of macroscopic and efficient data, but also reveals information on microstructures, strata, magmatic rock, and mineralization [95]. In this way, many types of ore-forming and ore-controlling elements can be reasonably determined. Research into the spectral combination, spectral testing, and spectral inversion of remote sensing data can be used to enhance and extract specific rock types, mineralization alteration types, and mineral types, and to improve high-resolution remote sensing prospecting technology and obtain research results that can be used for rapid and low investment [96]. Furthermore, combining geology with health, linking pollution research with environmental geology, or relating remote sensing to biogeochemistry are all worthy research fields[97], which could lead to better coupling of remote sensing surface information and geophysical data. Therefore, geological remote sensing research needs to be truly multidisciplinary and interdisciplinary, and geological surveys can be made more detailed and efficient through cross-linking with other disciplines.

4.3 Deep learning techniques in high-resolution remote sensing

Deep learning is a hot topic in machine learning and artificial intelligence, which imitates the mechanism of the human brain to interpret data. By training a large amount of data, deep learning can automatically obtain the relevant information and make a corresponding analysis and judgment, which can greatly improve the processing ability of high-resolution remote sensing images, thus enhancing their application value. Recently, research has been conducted on deep learning in geological hazard detection and remote sensing image recognition [98,99]. Table 6 presents recently published literature on deep learning applications employing high-spatial-resolution remote sensing data. It can be concluded that deep learning has good applications for image classification and scene classification but is less relevant to geology and other related fields. This is because most scene and image classification is based on artificial ground objects with geometric shape comparison rules that are easy to recognize and classify. Geological bodies are multi-type, multi-scale, multi-genesis, and multi-environment; therefore, it is very challenging to classify and recognize geological bodies from remote sensing images.

Table 6. Recent published literature on deep learning geology applications using HR data.

Research field	Author, publishing date	Paper topic	Data source	Resolution (m)	Related literature
Geological disaster	Ying & Linzhi, 2016	Geological disaster recognition	Google Earth	1	Geological disaster recognition on optical remote sensing images using deep learning
	Lee, 2007	Landslide susceptibility mapping	KOMPSAT-1	6.6	Landslide susceptibility mapping using an artificial neural network in the Gangneung area

 doi:10.20944/preprints201811.0162.v1

Author Contributions:

All authors made significant contributions to the manuscript. Chunming Wu, Xiao Li, Weitao Chen, Xianju Li conceived of, designed, and wrote the manuscript. Xiao Li and Weitao Chen revise the manuscript.

Acknowledgments:

This research was jointly supported by the Fundamental Research Funds for Central Universities, China University of Geosciences (Wuhan) (No.CUG170648), and Natural Science Foundation of China (No. 41701516).

References

1. Sultan, M.; Arvidson, R.E.; Sturchio, N.C. Mapping of serpentinites in the Eastern Desert of Egypt by using Landsat thematic mapper data. *Geology*. 1986, 14(12), 995-999, DOI: 10.1130/0091-7613(1986)14<995:MOSITE>2.0.CO;2.
2. Abrams, M.J.; Rothery, D.A.; Pontual, A. Mapping in the Oman ophiolite using enhanced Landsat Thematic Mapper images.*Tectonophysics*. 1988, 151(1), 387-401, DOI: 10.1016/0040-1951(88)90254-5.
3. Jutz, S.L.; Chorowicz, J. Geological mapping and detection of oblique extensional structures in the Kenyan Rift Valley with a SPOT/Landsat-TM datamerge Geology. *International Journal of Remote Sensing*. 1993, 14(9), 1677-1688, DOI: 10.1080/01431169308953994.
4. Sabins, F.F. Remote sensing for mineral exploration. *Ore Geology Reviews*. 1999 , 14(3–4), 157-183, DOI: 10.1016/S0169-1368(99)00007-4.
5. Singhroy, V.H.; Loehr, J.E.; Correa, A.C. Landslide risk assessment with high spatial resolution remote sensing satellite data. *IEEE Geoscience and Remote Sensing Symposium*. 2000, 6, 2501-2503, DOI: 10.1109/IGARSS.2000.859620.
6. Kruse, F.A.; Boardman, J.W.; Huntington, J.F. *IEEE Transactions on Geoscience & Remote Sensing*. 2003, 41(6), 1388-1400, DOI: 10.1109/TGRS.2003.812908.
7. Chipman, J.W.; Lillesand, T.M.; Schmaltz, J.E.; Leale, J.E.; Nordheim, M.J. Mapping lake water clarity with Landsat images in Wisconsin, U.S.A. *Canadian Journal of Remote Sensing*. 2004, 30(1), 1-7, DOI: 10.5589/m03-047.
8. Debba, P.; Ruitenbeek, F.J.A.V.; Meer, F.D.V.D.; Carranza, E.J.M.; Stein, A. Optimal field sampling for targeting minerals using hyperspectral data. *Photogrammetric Engineering & Remote Sensing*. 2005, 99(4), 373-386, DOI: 10.1016/j.rse.2005.05.005.
9. Yong, A.; Hough, S.E.; Cox, B.R.; Rathje, E.M.; Bachhuber, J. Seismic-zonation of Port-au-Prince Using Pixel- and Object-based Imaging Analysis Methods on ASTER GDEM. *Photogrammetric Engineering & Remote Sensing*. 2011, 77(9), 909-921, DOI: 10.14358/PERS.77.9.909.
10. Gei C.; Hannes Taubenbck; Wurm, M.; Esch, T.; Nast, M. Remote Sensing-Based Characterization of Settlement Structures for Assessing Local Potential of District Heat. *Remote Sensing.* 2011, 3(7), 1447-1471, DOI:10.3390/rs3071447.
11. Amer, R.; Kusky, T.; Mezayen, A.E. Remote sensing detection of gold related alteration zones in Um Rus area, Central Eastern Desert of Egypt. *Advances in Space Research.* 2012, 49(1), 121-134, DOI: 10.1016/j.asr.2011.09.024.
12. Markandeyulu, A.; Patra, I.; Raju, B.V.S.N.; Chaturvedi, A.K.; Parihar, P.S. Interpretation of aero-magnetic data and satellite imagery to delineate structure - a case study for uranium exploration from Gwalior Basin, India. *Journal of the Geological Society of India.* 2012, 80(3), 382-392, DOI: 10.1007/s12594-012-0156-2.
13. Alanazi, H.A.; Ghrefat, H.A. Spectral Analysis of Multispectral Landsat 7 ETM + and ASTER Data for Mapping Land Cover at Qurayah Sabkha, Northern Saudi Arabia. *Journal of the Indian Society of Remote Sensing.* 2013, 41(4), 833-844, DOI: 10.1007/s12524-013-0291-2.
14. Janati, M.E.; Soulaimani, A.; Admou, H.; Youbi, N.; Hafid, A. Application of ASTER remote sensing data to geological mapping of basement domains in arid regions: a case study from the Central Anti-Atlas, Iguerda inlier, Morocco. *Arabian Journal of Geosciences.* 2014, 7(6), 2407-2422, DOI: 10.1007/s12517-013-0945-y.
15. Kruse, F.A.; Kim, A.M.; Jalobeanu, A.; Olsen, R.C. Multispectral, hyperspectral, and LiDAR remote sensing and geographic information fusion for improved earthquake response. *Spie Defense + Security*. 2014, 9088, 90880K, DOI: 10.1117/12.2049725.
16. Madani, A.; Niyazi, B. Groundwater potential mapping using remote sensing techniques and weights of evidence GIS model: a case study from Wadi Yalamlam basin, Makkah Province, Western Saudi Arabia. *Environmental Earth Sciences.* 2015, 74(6), 1-14, DOI: 10.1007/s12665-015-4524-2.
17. Gabr, S.S.; Hassan, S.M.; Sadek, M.F. Prospecting for new gold-bearing alteration zones at El-Hoteib area, South Eastern Desert, Egypt, using remote sensing data analysis *Ore Geology Review*. 2015, 71 :1-13 . 2015, 71, 1-13, DOI: 10.1016/j.oregeorev.2015.04.021.
18. Sonbul, A.R.; El-Shafei, M.K.; Bishta, A.Z. Using Remote Sensing Techniques and Field-Based Structural Analysis to Explore New Gold and Associated Mineral Sites Around Al-Hajar Mine, Asir

Terrane, Arabian Shield. *Journal of African Earth Sciences.* 2016, 117, 285-302, DOI: 10.1016/j.jafrearsci.2016.02.009.

19. Vural, A.; Özsen Corumluoglu; Asri, I. Remote sensing technique for capturing and exploration of mineral deposit sites in Gumushane metallogenic province, NE Turkey. *Journal of the Geological Society of India.* 2017, 90(5), 628-633, DOI: 10.1007/s12594-017-0762-0.
20. Saadi, N.M.; Watanabe, K. Lineaments extraction and analysis in Eljufra area, Libya. *Journal of Applied Remote Sensing*. 2008, 1(4)347-366, DOI: 10.1117/1.2994727.
21. Raharimahefa, T.; Kusky, T.M. Structural and remote sensing studies of the southern Betsimisaraka Suture, Madagascar. *Gondwana Research.* 2006, 10 (1-2),186-197, DOI: 10.1016/j.gr.2005.11.022.
22. Koç, A.; Kaymakcı, N. Kinematics of Sürgü Fault Zone (Malatya, Turkey): A remote sensing study. *Journal of Geodynamics.* 2013, 65, 292-307, DOI: 10.1016/j.jog.2012.08.001.
23. Rodriguez, J.; Ustin, S.; Sandoval-Solis, S.; O'Geen, A.T. Food, water, and fault lines: Remote sensing opportunities for earthquake-response management of agricultural water. *Science of The Total Environment.* 2016, 565, 1020-1027, DOI: 10.1016/j.scitotenv.2016.05.146.
24. Ahmadi, H.; Das,A.; Pourtaheri, M.;Komaki, C.B. ; Khairy, H. Redefining the watershed line and stream networks via digital resources and topographic map using GIS and remote sensing (case study: the Neka River's watershed. *Natural Hazards*. 2014, 72(2), 711-722, DOI: 10.1007/s11069-014-1031-9.
25. Vaughan, R.G.; Kervyn, M.; Realmuto, V.; Abrams, M.; Hook, S.J. Satellite measurements of recent volcanic activity at Oldoinyo Lengai, Tanzania. *Journal of Volcanology and Geothermal Research.* 2008, 173(3), 196-206, DOI: 10.1016/j.jvolgeores.2008.01.028.
26. Bishop,C. A.; Liu, J.G.; Mason,P.J. Hyperspectral remote sensing for mineral exploration in Pulang, Yunnan Province, China. *International Journal of Remote Sensing*. 2011, 32 (9), 2409-2426, DOI: 10.1080/01431161003698336.
27. Crósta, A.P. ; De Souza Filho C.R.; Azevedo, F.; Brodie, C. Targeting key alteration minerals in epithermal deposits in Patagonia, Argentina, using ASTER imagery and principal component analysis. *International Journal of Remote Sensing.* 2003, 24(21), 4233-4240, DOI: 10.1080/0143116031000152291.
28. Cloutis, E.A. Review Article Hyperspectral geological remote sensing: evaluation of analytical techniques. *International Journal of Remote Sensing.* 1996, 17(12), 2215-2242, DOI: 10.1080/01431169608948770.
29. Meer, F.D.V.D. Imaging spectrometry for geological remote sensing. *Geologie en Mijnbouw.* 1998, 77(2), 137-151, DOI: 10.1023/A:1003538401892.
30. Meer, F.D.V.D.; Werff, H.M.A.V.D. ; Ruitenbeek, F.J.A.V.; Hecker, C.A.; Bakker, W.H. Multi- and hyperspectral geologic remote sensing: A review. *International Journal of Applied Earth Observation and Geoinformation.* 2011, 14(1), 112-128, DOI: 10.1016/j.jag.2011.08.002.
31. Meer, F.V.D.; Hecker, C.; Ruitenbeek, F.V.; Werff, H.V.D.; Wijkerslooth, C.D. Geologic remote sensing for geothermal exploration: A review. *International Journal of Applied Earth Observation and Geoinformation.* 2014, 33(1), 255-269, DOI: 10.1016/j.jag.2014.05.007.
32. Harris, J.R.; Rogge, D.; Hitchcock, R.; Ijewliw, O.; Wright, D. Mapping lithology in Canada's Arctic: application of hyperspectral data using the minimum noise fraction transformation and matched filtering. *Canadian Journal of Earth Sciences.* 2005, 42(12), 2173-2193, DOI: 10.1139/e05-064.
33. Pour, A.B.; Hashim, M. The application of ASTER remote sensing data to porphyry copper and epithermal gold deposits. *Ore Geology Reviews.* 2012, 44(1), 1-9, DOI: 10.1016/j.oregeorev.2011.09.009.
34. Zhang, T.T.; Liu, F. Application of hyperspectral remote sensing in mineral identification and mapping. *International Conference: Computer Science and Network Technology.* 2013, 103-106, DOI: 10.1109/ICCSNT.2012.6525900.
35. Li, Z.; Yang, R.; Dang, F.; Du, P.; Zhang, X. A review on the geological applications of hyperspectral remote sensingtechnology. *Hyperspectral Image & Signal Processing.* 2014, 1-4, DOI: 10.1109/WHISPERS.2012.6874235 .
36. Asadzadeh, S.; Roberto, D.S.F.C. A review on spectral processing methods for geological remote sensing. *International Journal of Applied Earth Observation and Geoinformation.* 2016, 173, 162-173, DOI: 10.1016/j.jag.2015.12.004.

37. Thomas, C.; Ranchin, T.; Wald, L.; Chanussot, J. Synthesis of Multispectral Images to High Spatial Resolution: A Critical Review of Fusion Methods Based on Remote Sensing Physics. *IEEE Transactions on Geoscience and Remote Sensing*. 2008, 46(5), 1301-1312, DOI: 10.1109/TGRS.2007.912448.
38. Zhao C.; Lu, Z. Remote Sensing of Landslides-A Review. *Remote Sensing*. 2018, 10(2), 279, DOI: 10.3390/rs10020279.
39. Toutin, T. Spatiotriangulation with multisensor VIR/SAR images. *Geoscience & Remote Sensing IEEE Transactions on.* 2004, 42(10), 2121-2129. 2001, DOI: 10.1109/TGRS.2004.834638.
40. Chen, W.; Li, X.; He, H.; Wang, L. A Review of Fine-Scale Land Use and Land Cover Classification in Open-Pit Mining Areas by Remote Sensing Techniques. *Remote Sensing*, 2017a, 10(1), 15, DOI: 10.3390/rs10010015.
41. Chen, W.; Li, X.; He, H.; Wang, L. Assessing Different Feature Sets' Effects on Land Cover Classification in Complex Surface-Mined Landscapes by ZiYuan-3 Satellite Imagery. *Remote Sensing*. 2017b, 10(1), 23, DOI: 10.3390/rs10010023.
42. Sonbul, A.R.; El-Shafei, M.K.; Bishta, A.Z. Using remote sensing techniques and field-based structural analysis to explore new gold and associated mineral sites around Al-Hajar mine, Asir terrane, Arabian Shield. *Journal of African Earth Sciences.* 2016, 117, 285-302, DOI: 10.1016/j.jafrearsci.2016.02.009.
43. Behnia, P. ; Harris, J. R.; Rainbird, R. H.; Williamson, M. C.; Sheshpari, M. Remote predictive mapping of bedrock geology using image classification of Landsat and SPOT data, western Minto Inlier, Victoria Island, Northwest Territories, Canada. *International Journal of Remote Sensing*. 2012, 33(21), 6876-6903, DOI: 10.1080/01431161.2012.693219.
44. Han, L.; Zhao, B.; Wu, J.J.; Zhang, S.Y.; Pilz, J. An integrated approach for extraction of lithology information using the SPOT 6 imagery in a heavily Quaternary-covered regionNorth Baoji District of China. *Geological Journal*. 2017, DOI: 10.1002/gj.3061.
45. Berthier, E.; Toutin,T. SPOT5-HRS digital elevation models and the monitoring of glacier elevation changes in North-West Canada and South-East Alaska. *Remote Sensing of Environment*. 2008, 112(5), 2443-2454, DOI: 10.1016/j.rse.2007.11.004.
46. Korona, J.; Berthier, E.; Bernard, M.; Remy, F.; Thouvenot, E. SPIRIT. SPOT 5 stereoscopic survey of Polar Ice: Reference Images and Topographies during the fourth International Polar Year (2007–2009). *Isprs Journal of Photogrammetry & Remote Sensing*. 2009, 64, 204-212, DOI: 10.1016/j.isprsjprs.2008.10.005.
47. Pieczonka, T.; Bolch,T.; Wei, J.; Liu, S. Heterogeneous mass loss of glaciers in the Aksu-Tarim Catchment (Central Tien Shan) revealed by 1976 KH-9 Hexagon and 2009 SPOT-5 stereo imagery. *Remote Sensing of Environment*. 2013, 130(4), 233-244, DOI: 10.1016/j.rse.2012.11.020.
48. Bouillon, A.; Bernard, M.; Gigord, P.; Orsoni, A.; Rudowski, V. SPOT 5 HRS geometric performances: Using block adjustment as a key issue to improve quality of DEM generation. *Isprs Journal of Photogrammetry & Remote Sensing*. 2006, 60(3), 134-146, DOI: 10.1016/j.isprsjprs.2006.03.002.
49. Kornus,W.; Alamús, R.; Ruiz, A.; Talaya, J. DEM generation from SPOT-5 3-fold along track stereoscopic imagery using autocalibration. *Isprs Journal of Photogrammetry & Remote Sensing*. 2006, 60(3), 147-159, DOI: 10.1016/j.isprsjprs.2005.12.004.
50. Ahmadi, H.; Das,A.; Pourtaheri, M.; Khairy, H.; Komaki,B.C. Redefining the Border line of the Neka River's Watershed with Comparing ASTER, SRTM, Digital Topography DEM, and Topographic Map by GIS and Remote Sensing Techniques. *Natural Hazards*. 2014 , 72 (2) :711-722, DOI: 10.1007/s11069-014-1031-9.
51. Sato, H.P.; Hasegawa, H.; Fujiwara, S.; Tobita, M.; Koarai, M. Interpretation of landslide distribution triggered by the 2005 Northern Pakistan earthquake using SPOT 5 imagery. *Landslides*. 2007, 4(2), 113-122, DOI: 10.1007/s10346-006-0069-5.
52. Chang, K. Comparison between automated and manual mapping of typhoon-triggered landslides from SPOT-5 imagery. *International Journal of Remote Sensing*. 2007, 28(8), 1843-1856, DOI: 10.1080/01431160600935638.
53. Kang, T.J.; Zhang, X.C.; Wang, H.Y. Assessment of the fused image of multispectral and panchromatic images of SPOT5 in the investigation of geological hazards. *Science in China*. 2008, 51(2), 144-153, DOI: 10.1007/s11431-008-6015-0.

54. Z.; Zhang, J. Interpretation of Landslide from SPOT-5 Imageries in the Three Gorges Reservoir Area. *International Workshop on Earth Observation and Remote Sensing Applications*. 2008, 1-5, DOI: 10.1109/EORSA.2008.4620291.
55. Bivic, R.L.; Allemand, P.; Quiquerez, A.; Delacourt, C. Potential and Limitation of SPOT-5 Ortho-Image Correlation to Investigate the Cinematics of Landslides: The Example of ``Mare à Poule d'Eau'' (Réunion, France). *Remote Sensing*. 2017, 9(2), 106, DOI: 10.3390/rs9020106.
56. Li, X.; Wang, P.; Zang, Y.B. Application of SPOT 5 Data Fusion on Investigating the Ecological Enviroment of Mining Area. *Urban Remote Sensing Event.* 2009, 1-6, DOI: 10.1109/URS.2009.5137594.
57. Harbi, H.; Madani, A. Utilization of SPOT 5 data for mapping gold mineralized diorite-tonalite intrusion, Bulghah gold mine area, Saudi Arabia. *Arabian Journal of Geosciences*. 2014, 7(9), 3829-3838, DOI: 10.1007/s12517-013-1035-x.
58. Mezned, N.; Mechrgui, N.; Abdeljaouad, S. Mine Wastes Environmental Impact Mapping Using Landsat ETM+ and SPOT 5 Data Fusion in the North of Tunisia. *Journal of the Indian Society of Remote Sensing*. 2016, 44(3), 1-5, DOI: 10.1007/s12524-015-0505-x.
59. Kruse, F.A.; Perry, S.L. Mineral Mapping Using Simulated Worldview-3 Short-Wave-Infrared Imagery. *Remote Sensing*. 2013, 5(6), 2688-2703, DOI: 10.3390/rs5062688.
60. Kruse, F.A.; Baugh, W.M.; Perry, S.L. Validation of DigitalGlobe WorldView-3 Earth imaging satellite shortwave infrared bands for mineral mapping. *Journal of Applied Remote Sensing*. 2015, 9(1) , 307-310, DOI: 10.1117/1.JRS.9.096044.
61. Monsef, A.E.; Khalifa, I.H.; Faisal, M. Mapping of hydrothermal alteration zones associated with potential sulfide mineralization using the spectral linear unmixing technique and WorldView II images at Wadi Rofaiyed, South Sinai, Egypt. *Arabian Journal of Geosciences*. 2015, 8(11), 1-16, DOI: 10.1007/s12517-015-1909-1.
62. Ye, B.; Tian, S.; Ge, J.; Sun, Y. Assessment of WorldView-3 Data for Lithological Mapping. *Remote Sensing*. 2017, 9(11), 1132, DOI: 10.3390/rs9111132.
63. Salati, S.; Ruitenbeek, F. V. ; Freek, V.D.M.; Naimi, B. Detection of Alteration Induced by Onshore Gas Seeps from ASTER and WorldView-2 Data. *Remote Sensing*. 2014, 6(4), 3188-3209, DOI: 10.3390/rs6043188.
64. Sefercik, U.G.; Alkan, M.; Buyuksalih, G.; Jacobsen, K. Generation and Validation of High-Resolution DEMs from Worldview-2 Stereo Data. *Photogrammetric Record*. 2013, 28(144), 362–374, DOI: 10.1111/phor.12038.
65. Oikonomidis, D.; Vavelidis, M.; Melfos, V.; Artashova, M. Searching for ancient gold mines in Filippoi area, Macedonia, Greece, using Worldview-2 satellite imagery. *Geocarto International*, 2015, 32(1), 87-96, DOI: 10.1080/10106049.2015.1128487.
66. Armstrong, W.H.; Anderson, R.S.; Allen, J.; Rajaram, H. Modeling the WorldView-derived seasonal velocity evolution of Kennicott Glacier, Alaska. *Journal of Glaciology*. 2016, 62(234), 1-15, DOI: 10.1017/jog.2016.66.
67. Fieber, K.D.; Mills, J.P.; Miller, P.E.; Clarke, L.; Ireland, L. Rigorous 3D change determination in Antarctic Peninsula glaciers from stereo WorldView-2 and archival aerial imagery. *Remote Sensing of Environment*. 2018, 205, 18-31, DOI: 10.1016/j.rse.2017.10.042.
68. Sun, Y.; Tian, S.; Di, B. Extracting mineral alteration information using WorldView-3 data. *Geoscience Frontiers*. 2017, 8, 1051-1062, DOI: 10.1016/j.gsf.2016.10.008.
69. Hu, W.; Wu, L.; Zhang, W.; Liu, B.; Xu, J. Ground Deformation Detection Using China's ZY-3 Stereo Imagery in an Opencast Mining Area. *ISPRS International Journal of Geo-Information.* 2017, 6(11), 361, DOI: 10.3390/ijgi6110361.
70. Fratarcangeli, F.; Murchio, G.; Rita, M.D.; Nascetti, A.; Capaldo, P. Digital surface models from ZiYuan-3 triplet: performance evaluation and accuracy assessment. *International Journal of Remote Sensing*. 2016, 37(15) ,1-27, DOI: 10.1080/01431161.2016.1192308.
71. Li, X.; Chen, W.; Cheng, X.; Wang, L. A Comparison of Machine Learning Algorithms for Mapping of Complex Surface-Mined and Agricultural Landscapes Using ZiYuan-3 Stereo Satellite Imagery. *Remote Sensing*, 2016, 8(6), 514, DOI: 10.3390/rs8060514.
72. Meer, F.D.V.D.; Werff, H.M.A.V.D.; Ruitenbeek, F.J.A.V. Potential of ESA's Sentinel-2 for geological applications. *Remote Sensing of Environment*. 2014, 148(148), 124-133, DOI: 10.1016/j.rse.2014.03.022.

73. Paul, F.; Winsvold, S.; Kääb, A.; Nagler, T.; Schwaizer, G. Glacier Remote Sensing Using Sentinel-2. Part II: Mapping Glacier Extents and Surface Facies, and Comparison to Landsat 8. *Remote Sensing*. 2016, 8(7), 575, DOI: 10.3390/rs8070575.
74. Kääb, A.; Winsvold, S.; Altena, B.; Nuth, C.; Nagler, T. Glacier Remote Sensing Using Sentinel-2. Part I: Radiometric and Geometric Performance, and Application to Ice Velocity. *Remote Sensing*. 2016, 8(7), 598, DOI: 10.3390/rs8070598.
75. Mielke, C.; Boesche, N.; Rogass, C.; Kaufmann, H.; Gauert, C. Spaceborne Mine Waste Mineralogy Monitoring in South Africa, Applications for Modern Push-Broom Missions: Hyperion/OLI and EnMAP/Sentinel-2. *Remote Sensing*. 2014, 6(8), 6790-6816, DOI: 10.3390/rs6086790.
76. Transon, J.; D'Andrimont, R.; Maugnard, A.; Defourny, P. Survey of Hyperspectral Earth Observation Applications from Space in the Sentinel-2 Context. *Remote Sensing*. 2018, 10(2), 157, DOI: 10.3390/rs10020157.
77. Park, S.E. Variations of Microwave Scattering Properties by Seasonal Freeze/Thaw Transition in the Permafrost Active Layer Observed by ALOS PALSAR Polarimetric Data. *Remote Sensing*. 2015, 7(12) , 17135-17148, DOI: 10.3390/rs71215874.
78. Saepuloh, A.; Koike, K.; Urai, M.; Sumantyo, J.T.S. Identifying Surface Materials on an Active Volcano by Deriving Dielectric Permittivity From Polarimetric SAR Data. *IEEE Geoscience & Remote Sensing Letters*. 2015, 12(8), 1620-1624, DOI: 10.1109/LGRS.2015.2415871.
79. Feng, G.; Jónsson, S.; Klinger, Y. Which Fault Segments Ruptured in the 2008 Wenchuan Earthquake and Which Did Not? New Evidence from Near-Fault 3D Surface Displacements Derived from SAR Image Offsets. *Bulletin of the Seismological Society of America*. 2017, 107(3), DOI: 10.1785/0120160126.
80. Tseng, K.H.; Kuo, C.Y.; Lin, T.H.; Huang, Z.C.; Lin, Y.C. Reconstruction of time-varying tidal flat topography using optical remote sensing imageries. *Isprs Journal of Photogrammetry & Remote Sensing*. 2017, 131, 92-103, DOI: 10.1016/j.isprsjprs.2017.07.008.
81. Ng, H.M.; Ge, L.; Du, Z.; Wang, S.; Ma, C. Satellite radar interferometry for monitoring subsidence induced by longwall mining activity using Radarsat-2, Sentinel-1 and ALOS-2 data. *International Journal of Applied Earth Observation & Geoinformation*. 2017, 61, 92-103, DOI: 10.1016/j.jag.2017.05.009.
82. Sun, Y.; Jiang, L.; Liu, L.; Sun, Q.; Wang, H. Mapping Glacier Elevations and Their Changes in the Western Qilian Mountains, Northern Tibetan Plateau, by Bistatic InSAR. *IEEE Journal of Selected Topics in Applied Earth Observations & Remote Sensing*, 2017, PP(99), 1-11, DOI: 10.1109/JSTARS.2017.2764751.
83. Béjarpizarro, M.; Carrizo, D.; Socquet, A.; Armijo, R.; Barrientos, S. Asperities and barriers on the seismogenic zone in North Chile: state-of-the-art after the 2007 Mw 7.7 Tocopilla earthquake inferred by GPS and InSAR data. *Geophysical Journal International*. 2010, 183(1), 390-406, DOI: 10.1111/j.1365-246X.2010.04748.x.
84. Salvi, S.; Tolomei, C.; Boncori, J.P.M.; Pezzo, G.; Atzori, S. Activation of the SIGRIS monitoring system for ground deformation mapping during the 2012 Emilia seismic sequence, using COSMO-SkyMed InSAR data. *Annals of geophysics = Annali di geofisica*. 2012, 55(4), 797-802, DOI: 10.4401/ag-6181.
85. Sun, L.; Muller, J.P. Evaluation of the Use of Sub-Pixel Offset Tracking Techniques to Monitor Landslides in Densely Vegetated Steeply Sloped Areas. *Remote Sensing*, 2016, 8(8), 659, DOI: 10.3390/rs8080659.
86. Lunden, B.; Wang, G. A GIS based analysis of data from Landsat TM, airborne geophysical measurements, and digital maps for geological remote sensing in the Stockholm region, Sweden. *International Journal of Remote Sensing*. 2001, 22(4), 517-532, DOI: 10.1080/01431160050505838.
87. Lamontagne, M.; Keating, P.; Perreault, S. Seismotectonic characteristics of the Lower St. Lawrence Seismic Zone, Quebec: insights from geology, magnetics, gravity, and seismics. *Canadian Journal of Earth Sciences*. 2003, 40(2), 317-336, DOI: 10.1139/e02-104.
88. Chen, S.; Zhou, Y. Classifying depth-layered geological structures on Landsat TM images by gravity data: a case study of the western slope of Songliao Basin, northeast China. *International Journal of Remote Sensing*. 2005, 26(13), 2741-2754, DOI: 10.1080/01431160500104210.

89. Yassaghi, A. Integration of Landsat imagery interpretation and geomagentic data on verification of deep-seated transverse fault lineaments in SE Zagros, Iran. *International Journal of Remote Sensing*. 2006, 27(20), 4529-4544, DOI: 10.1080/01431160600661283.
90. Saadi, N.M.; Aboud, E.; Saibi, H.; Watanabe, K. Integrating data from remote sensing, geology and gravity for geological investigation in the Tarhunah area, Northwest Libya. *International Journal of Digital Earth*. 2008, 1(4), 347-366, DOI: 10.1080/17538940802435844.
91. Saadi, N.M.; , A.; Saibi, H.; Watanabe, K. Integrating potential fields with remote sensing data for geological investigations in the Eljufra area of Libya. *Earth, Planets and Space*. 2008, 60(6), 539-547, DOI: 10.1186/BF03353116.
92. Saadi, N.M.; , A.; Saibi, H.; Watanabe, K. Integrated remote sensing data utilization for investigating structural and tectonic history of the Ghadames Basin, Libya. *International Journal of Applied Earth Observation & Geoinformation*. 2011, 13(5), 778-791, DOI: 10.1016/j.jag.2011.05.016.
93. Ma, Y.; Wu, H.; Wang, L.; Huang, B.; Ranjan, R. Remote sensing big data computing: Challenges and opportunities. *Future Generation Computer Systems*. 2015, 51, 47-60, DOI: 10.1016/j.future.2014.10.029.
94. Zhang, J.; Wu, C.; Wang, L. A Conceptual Framework for the Automated Generalization of Geological Maps Based on Multiple Agents and Workflow. *IEEE Access*. 2017, 4(99), 6374-6385, DOI: 10.1109/ACCESS.2016.2594259.
95. Pour, A.B.; Hashim, M. Identifying areas of high economic-potential copper mineralization using ASTER data in the Urumieh–Dokhtar Volcanic Belt, Iran. *Advances in Space Research*. 2012, 49(4), 753-769, DOI: 10.1016/j.asr.2011.11.028.
96. Zhan, Y.; Hu, G.; Wu,Y. The Feature Selection and Extraction of Hyperspectral Mineralization Information Based on Rough Sets Theory. *Workshop on Computational Intelligence & Industrial Application*. 2008 , 22(7), 282-286, DOI: 10.1109/PACIIA.2008.35.
97. Ma, Y. Remote sensing research in biogeochemistry of the Hetai gold deposit, Guangdong Province, China. *International Journal of Remote Sensing*. 2004, 25(2), 437-453, DOI: 10.1080/0143116031000102467.
98. Liu, Y.; Wu, L. Geological Disaster Recognition on Optical Remote Sensing Images Using Deep Learning. *Procedia Computer Science*. 2016, 91, 566–575, DOI: 10.1016/j.procs.2016.07.144.
99. Liu, P.; Choo, Kim-Kwang Raymond ; Wang, L.; Huang, F. SVM or deep learning? A comparative study on remote sensing image classification. *Soft Computing*. 2017, 21(23), 1-13, DOI: 10.1007/s00500-016-2247-2.